FISEVIER

Contents lists available at ScienceDirect

Journal of Non-Newtonian Fluid Mechanics

journal homepage: www.elsevier.com/locate/jnnfm





The benefits of a formalism built on recovery: Theory, experiments, and modeling

Jiachun Shi, Simon A. Rogers*

Department of Chemical and Biomolecular Engineering, University of Illinois at Urbana-Champaign, Urbana, 61801, United States of America

ARTICLE INFO

Keywords: Nonlinear viscoelasticity Theory Rheological measurements Constitutive model Wormlike micelles Time-resolved rheology

ABSTRACT

A new rheological formalism based on the ideas of recovery is presented. Our new formalism contains recoverable and unrecoverable contributions to arbitrary deformations. The introduction of the two displacement gradients leads to two distinct measures of strain and strain rates, which highlights the importance of performing recovery experiments. Having established the new formalism, we show the benefits of this way of thinking by performing transient step strain and startup shear recovery measurements in a wide range of shear strains and shear rates on a model viscoelastic solution. With recovery, we show clear similarities in the material behavior between the two test protocols. The resultant recovery material functions – recoverable modulus and flow viscosity – allow the development of a new constitutive model, which consists of nonlinear elastic and viscous functions, along with a retarded viscous term. The predictions of the model are compared favorably with the experimental data, including responses to extremely large step strains. These observations allow us to revisit the transient entanglement length, relaxation time, and damping function based on the idea of recovery rheology. The present findings suggest a clear correlation exists between microstructural evolution and recoverable and unrecoverable components and provide a new direction for the exploration of the relation between recovery material functions and material responses under different dynamic flows.

1. Introduction

Complex fluids continue to be heavily used in the food industry, biological applications, electronic and optical devices, and the plastics industry, among others [1]. The microstructures of complex fluids under different thermal and deformation histories affect their rheological responses [1]. Complex fluids are not readily classified as either Hookean elastic solids nor Newtonian viscous fluids. Instead, complex fluids have mechanical properties that are intermediate between the two, making them viscoelastic. At infinitesimal deformations, complex fluids approach the two extreme cases characterized by the classical theories of elasticity and hydrodynamics. The theory of elasticity concerns the recoverable storage of energy of solids and relates the stress to infinitesimal strains. In comparison, the theory of hydrodynamics focuses on the energetically dissipative viscous properties of liquids that relate stresses to shear rates linearly [2]. Complex fluids are able to simultaneously store and dissipate energy, giving rise to the complexity of their transient responses. Various rheological constitutive models have been developed to describe the relations between stress, strain, and time related to industrial processes [2]. The development of such constitutive relations heavily impacts the design of rheological protocols for obtaining relevant model parameters and predicting material behaviors.

The development of viscoelastic constitutive models started from the studies of polymeric systems, given their remarkable viscoelastic mechanical properties. Extensive discussions of polymeric dynamics have been presented [2-6]. To study the dynamics of complex fluids, researchers often start with generalized Newtonian fluid dynamics and continuum assumptions to make general mathematical modeling and analysis feasible. Theories have been proposed to describe the local behavior of the motion at points in the continuous medium [7]. The local dynamics of the material points are characterized by the local configurations, which are represented by the deformation functions. Two classical deformation functions are typically relied on to describe the deformation: the deformation gradient tensor [1,4,8] and the displacement gradient tensor [6,9]. Both functions quantify the transition of an infinitesimal line in a solid body, and the identity matrix mathematically relates the two functions. A typical representation of the displacement gradient tensor can be referred to the work by Tschogel in Section 1 [6]. The relative changes in displacement of the infinitesimal line between a reference time t and the current time t' are represented by the strain tensor. The rates of change in displacement of the infinitesimal line between the reference time t and the current

^{*} Corresponding author.

E-mail address: sarogers@illinois.edu (S.A. Rogers).

time t' are used to define the velocity gradient tensor and rate-ofstrain tensor [2]. This understanding has influenced the development of most rheological models and shaped the discussion of designing and performing rheometric experiments. The reference configuration invoked when deriving the strain and rate of strain tensors is usually taken at a reference time t = 0 in which the material is unrotated and unstretched [10,11].

While viscoelastic liquids behave as viscous liquids under steady flow conditions, they also have properties of elastic solids, and they have long been known to recover some or all of the acquired deformation upon load release [12-16]. The idea of recovery rheology was proposed by Weissenberg [17] to link recoverable strain with normal stresses and shear stress. Philippoff [18] later studied the correlation of recoverable shear strain with properties of polymer solutions, and Reiner [19] even regarded the recoverable deformation as the definition of strain. The separation of recoverable strain allowed Reiner, as commented by Oldroyd, to "isolate, for separate treatment, linearity, parametric non-linearity, deformational nonlinearity and tensorial non-linearity in equations of state" [20]. Recent work has shown promising correlations between mechanical properties of materials, including polymer-like micelles [21-23], yield-stress materials [24-26], and thixotropic materials [27] observed under applications of different deformations and microstructural evolution using recoverable strains determined by constrained recovery measurements.

A constrained recovery measurement involves application of a stress or strain to a material initially at rest and in a stress-free state. Weissenberg referred to this state as the "ground state" of the material, though we prefer the language of being in a state of global or local equilibrium. After application of the stress or strain protocol for an experimental time t_{exp} , a step often referred to as the recovery step is applied, in which the shear stress is removed, as depicted in Fig. 1(a). It is important to notice that the constrained part of the recovery step means that only the shear stress is set to zero, while the other components of the stress tensor are allowed to evolve. The material remains constrained in the geometry at a fixed height under shear deformation. During the recovery step, the material is allowed to drift back into equilibrium, which may or may not be the same state from which it was initially perturbed. The amount of strain recovered in this stress-free step is the recoverable strain, which is a function of two times, the time during which the initial protocol ran and the time under constrained recovery, $\gamma_{rec}(t_{exp}, t_{rec})$. Similarly, the position the material recovers to is the unrecoverable strain, which is a function of the same two times $\gamma_{unrec}(t_{exp}, t_{rec})$. In this paper, we will generally use the ultimate recoverable and unrecoverable strains $\gamma_{rec}(t) = \gamma_{rec}(t_{exp}, t_{rec} \rightarrow t_{exp})$ ∞) and $\gamma_{unrec}(t) = \gamma_{unrec}(t_{exp}, t_{rec} \rightarrow \infty)$. Recovery rheology acknowledges two distinct and measurable strain components, and therefore also identifies two shear rates representing the rates at which strain is acquired recoverably and unrecoverably, $\dot{\gamma}_{rec}(t)$ and $\dot{\gamma}_{unrec}(t)$.

Because the definitions used in traditional rheology allow for (or require) the reference state to be defined by the observer, we refer to this as the *anthropocentric* view. In contrast, recovery rheology 'asks' the material where the new reference state is at each moment. We use the greek *ylikó*, meaning *material* to refer to recovery rheology as being *ylikócentric*, removing the importance from choices made by the observer and placing the emphasis on the determination of material equilibrium states.

Previous investigations have already shown that the final equilibrium state reached by the material after releasing the load to zero is not necessarily the same as the initial state. A general treatment must therefore allow for the movement of the equilibrium state. The concept of recovery can be visualized as presented as Fig. 1(b) when considering the shear deformation of a cube of material at the reference time t, with the same concept applied at the later time t'. The cube can be displaced to a new state defined by material equilibrium properties alone after releasing the stress. Given that inelastic fluids display no recovery, the

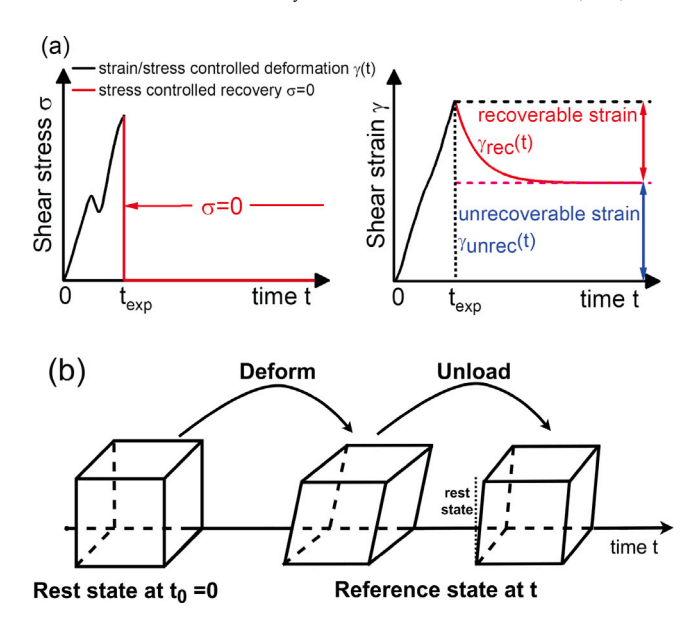


Fig. 1. Illustration of constrained recovery protocol (a) left: stress versus time and right: shear strain versus time for a given stress/stress-controlled deformation applied for a period of 0 < t <experimental time t_{exp} and subsequent unloading of the material (shear stress $\sigma = 0$). Representation of recovery rheology (b) when considering the shearing deformation of a material cube and selecting the reference time t as an example.

formalism of the displacement gradient tensor based on fluid dynamics does not account for the recovery of strain.

To address the potential incompleteness that exists in the conventional definition of the displacement gradient tensor, we go back to the observation that viscoelastic liquids display recovery and invoke the idea that where the material recovers to is the new equilibrium state. Oldroyd defined the equilibrium state as the state obtained if any material motion is instantaneously stopped, and the stresses remaining at zero velocity were reduced reversibly to zero [28]. The idea of the stress-free material equilibrium state has been explored in solid mechanics, mainly for materials that exhibit elasto-viscoplastic deformation in dynamic loading [29]. In that case, the stress-free state resulting from the unloading process is referred to as the intermediate configuration, separated from either the reference or current configurations. However, this stress-free state is somewhat fictitious in plastic solids due to the heterogeneous micromechanical structure that results from an inability of all material points to reach stressfree states simultaneously [29]. The relevant mathematical derivations for distinguishing elastoplastic and viscoplastic behaviors following the multiplicative decomposition of deformation gradient tensor [30, 31] do not have any physical meaning because of the fictitious intermediate configuration. The idea of multiplicative decomposition has recently been utilized for modeling the yield-stress fluids and a complete 3-dimensional form of the kinematic hardening model was proposed [32]. The intermediate structural space is associated with the Mandel stress [33], with the setup that the reference state is the undeformed body, and the current state is the deformed body.

Rajagopal and co-workers have published a series of papers on developing a general thermodynamic framework to model the behaviors of viscoelastic fluids that are isotropic [34], and anisotropic [35] based on deformation gradient tensor. Later, they extended the framework to model the fiber-spinning process [36]. In their thermodynamic framework, the "current" natural configuration, which can be represented by the stress-free configuration, was introduced with respect to current time t'. The presence of the natural configuration gave rise to two deformation gradient tensors that describe the mapping from "current natural configuration" to the current configuration and from reference configuration to "current natural configuration", respectively, in theory

development [34,35]. Limited discussions were presented on how to transfer theoretical understandings into experimental design.

In this paper, we attribute the natural configuration as the stress-free material equilibrium state and recognize that both the reference and current configurations have corresponding stress-free states. The schematic is shown as Fig. 2 in Section 2. The allowance removes any specific choice regarding where to define the reference configuration from the experimenter. Rather, we allow the material to reveal its new equilibrium. For large deformations imposed over long times, which closely resemble industrial processing conditions, using the initial configuration as the reference state lacks clear meaning due to the fading memory of the material [9]. This representation can be found in Fig. 1(b), where we draw clear distinctions between initial or rest configuration and reference configuration. The two stress-free states introduce two displacement gradient tensors with physical meanings that allow clear distinctions regarding elastic and viscous contributions in a transient manner.

Acknowledging the two components of the strain and the rate is more than an analytical step in theory development. It means that experiments are required that are capable of determining both components. While modern rheological protocols vary the total strain or rate in different manners, a subtle but important change can be made to them that allows researchers to know the evolution of both components of the strain and rate. The change necessitates an iterative experimental paradigm that determines how far from equilibrium materials are at any given moment during a prescribed protocol, and to where the equilibrium state has moved. The results of such experiments provide more detailed data than traditional experiments that determine bulk behaviors in terms of the composite parameters. These more detailed data sets can, in turn, be used to construct new constitutive models.

Many constitutive models can be represented by mechanical analogs comprised of combinations of springs and dashpots [5]. The Maxwell and Kelvin–Voigt models are the simplest descriptions of viscoelastic liquids and solids. The Maxwell model can be represented by a Hookean spring and a Newtonian dashpot in series, and the Kelvin–Voigt model can be represented by a spring and a dashpot in parallel. While the Maxwell and Kelvin–Voigt models account for some behaviors, they are over-simplifications of the dynamic behavior of many complex systems, which require more complicated models, such as the Graham, Likhtman, and Milner, McLeish (GLaMM) model [37]. As we show in this work, recovery rheology provides more information than traditional approaches, simultaneously allowing for more detailed comparisons to constitutive models to be made, as well as the development of new models.

Recovery rheology requires revision of the definitions of material functions. In recovery rheology, recoverable strain is due to elastic processes while unrecoverable strain is due to plastic or viscous processes. Because only one of these is associated with elastic properties, recovery rheology has one natural modulus, the recoverable modulus, G_{rec} , [21,22,38] which is defined as the ratio of the stress to the ultimate recoverable strain,

$$G_{rec}(t) = \frac{\sigma(t)}{\gamma_{rec}(t)}. (1)$$

It can be seen from Eq. (1) that the recoverable modulus is the inverse of the recoverable compliance, $J_e(t)$, which is also known as the steady state compliance from creep tests. While only the recoverable strain is associated with elastic processes, both recoverable and unrecoverable strain rates lead to viscous responses. These definitions are direct analogies to the Maxwell and Kelvin–Voigt models. Based on the rates at which recoverable and unrecoverable strain are acquired, $\dot{\gamma}_{rec}$ and $\dot{\gamma}_{unrec}$, we define the flow viscosity, η_{flow} , and the retardation viscosity, η_{ret} ,

$$\eta_{flow}(t) = \frac{\sigma(t)}{\dot{\gamma}_{unrec}(t)},\tag{2}$$

and

$$\eta_{ret}(t) = \frac{\sigma(t)}{\dot{\gamma}_{rec}(t)}.\tag{3}$$

Recent works [21,22] have reported observations of the recoverable and unrecoverable contributions in soft matter systems. It is been shown that the recoverable modulus and flow viscosity, G_{rec} and η_{flow} , can be directly related to microstructural evolution throughout rheological tests that probe linear and nonlinear behaviors.

In this work, we also pay attention to the relaxation time and the damping function. The relaxation time, λ , is the characteristic timescale for the material to relax from the deformed state to the equilibrium state [4]. The relaxation time can be determined from the frequency at which the dynamic moduli cross in an oscillatory test carried out in the linear viscoelastic regime. It remains an open question as to how to define a relaxation time characterizing the dynamics of viscoelastic materials under large or nonlinear deformations. For example, Yamamoto proposed a rate-dependent relaxation time spectrum to describe nonlinear viscoelastic phenomenon [39]. However, this approach requires a rational form of the relaxation spectrum to be given beforehand. The damping function, $h(\gamma_0)$, was first introduced by Wagner to generalize the rubber-like liquid theory that is used for describing polymer fluids [8] by correcting the assumption that the flow does not affect the rate of deformation [40]. Following network disentanglement theories, the damping function is defined physically as the survival probability of the network after imposing a step strain, depending only on the deformation [41]. When the damping function is close to 1, the imposed deformation is small and the network remains largely intact. In this circumstance, the network undergoes nearly purely elastic deformation, and the process is entirely recoverable. By contrast, when the damping function approaches 0 at the very largest deformations, entanglements are removed, and no network exists in the system [42]. We take another look at these two material functions from the perspective of recovery rheology for generalizing viscoelastic responses in both linear and nonlinear regimes under the application of different deformations.

In the current study, we revisit the definition of the displacement gradient tensor to incorporate the recoverable behaviors observed by viscoelastic materials. This revised construction takes the *yilkó-centric* view of deformation by acknowledging the existence of the material equilibrium stress-free state and provides a framework to understand both linear and nonlinear material responses in the language of recovery rheology.

After a discussion of the displacement gradient and the connection to recovery material metrics, we present detailed step strain and startup shear recovery measurements for a wide range of strain amplitudes and shear rates on a model viscoelastic material and observe clear correlations between the two distinct test protocols. On the basis of our recovery rheology experimental results, we propose a new constitutive model and compare its predictions to the experimental observations. We also revisit the concepts of relaxation time and damping functions based on the concepts of recovery rheology to infer more information on the microstructural changes leading to deviations from the linear response.

The work is summarized as follows: In Section 2, we revisit the definition of the displacement gradient tensor, which is then applied to design the constrained recovery experimental protocols in Section 3, along with the outline of material preparation (Section 3.1) and experimental procedures (Section 3.2). The results of the experiments are discussed in Section 4, including the viscoelastic characterizations (Section 4.1), the development of a constitutive model based on recovery material functions determined from two recovery measurements (Section 4.2), and, finally, the revision in concepts of relaxation time and damping function in the framework of recover rheology (Section 4.3). Finally, conclusions are presented in Section 5.

2. Reconstruction of the displacement gradient tensor

We combine the traditional construction of displacement gradient tensor and the experimental observations of viscoelastic fluids to develop the reconstruction as represented in Fig. 2. The set of the unit vectors $\widehat{x_1}$, $\widehat{x_2}$, $\widehat{x_3}$ is used to define the position vectors in the Cartesian coordinate. At some reference time t, two infinitesimal material particles X_1 and X_2 are separated by a relative distance represented by

$$\overrightarrow{X_1 X_2} = dr_i. (4)$$

Each of the particles has a stress-free equilibrium state given by X_{1e} and X_{2e} , respectively. These are the points each particle would recover to if all stresses were removed. If the whole material body is at equilibrium, the material particles and their equilibrium positions will coincide. The distances from each particle to their associated equilibrium states are

$$\overrightarrow{X_1 X_{1e}} = dr_{ef,1i}, \overrightarrow{X_{2e} X_2} = dr_{ef,2i}. \tag{5}$$

The displacement between X_{1e} and X_{2e} is given by

$$\overrightarrow{X_{1e}X_{2e}} = dr_{eq.i}. ag{6}$$

In Eqs. (5) and (6) and for the rest of this discussion, we use subscripts f and o to represent displacement from and displacement of the equilibrium state. Because neither particle is aware of the equilibrium state of the other, no position vectors can be drawn between the pairs X_1 and $X_{2,e}$, or X_2 and $X_{1,e}$. At the current time t', in configuration $B_{t'}$, the two particles have become displaced to new locations X_1' and X_2' owing to the application of load experienced by the continuum medium, with the new relative distance

$$\overline{X_1'X_2'} = dr_i'. \tag{7}$$

The two stress-free equilibrium states are also displaced, to new positions X_{1e}' and X_{2e}' . The relative distances from particles to their equilibrium states are now

$$\overrightarrow{X_1'X_{1e}'} = dr'_{ef,1i}, \overrightarrow{X_{2e}'X_2'} = dr'_{ef,2i}.$$
 (8)

The relative distances between two X'_{1e} and X'_{2e} are denoted by

$$\overline{X'_{1e}X'_{2e}} = dr'_{eo.i}. (9)$$

Here, the motion of the equilibrium state from time t to t' is the primary concern. The directions of each position vector only serve to provide the mathematical representations of the vectors. For X'_{1e} and X'_{2e} , as seen in Fig. 2, we have

$$\overline{X_{1e}X'_{1e}} = u_{eo,i}(r_{eo,i}),$$
 (10)

and

$$\overline{X_{2e}X_{2e}'} = u_{eo,i}(r_{eo,i} + dr_{eo,i}).$$
 (11)

We further have

$$u_{eo,i}(r_{eo,i}) + dr'_{eo,i} = dr_{eo,i} + u_{eo,i}(r_{eo,i} + dr_{eo,i}),$$
(12)

which can be arranged to

$$dr'_{eo,i} = dr_{eo,i} + u_{eo,i}(r_{eo,i} + dr_{eo,i}) - u_{eo,i}(r_{eo,i}).$$
(13)

By assuming infinitesimal deformation, we use Taylor's series to expand the term $u_{eo,i}(r_{eo,i}+dr_{eo,i})$

$$u_{eo,i}(r_{eo,i} + dr_{eo,i}) = u_{eo,i}(r_{eo,i}) + dr_{eo,j} \frac{\partial u_{eo,i}(r_{eo,i})}{\partial r_{eo,j}}$$
(14)

+ higher order terms.

in which the higher order terms can be ignored. Finite strain requires a more complicated formalism to account for nonlinear responses, and

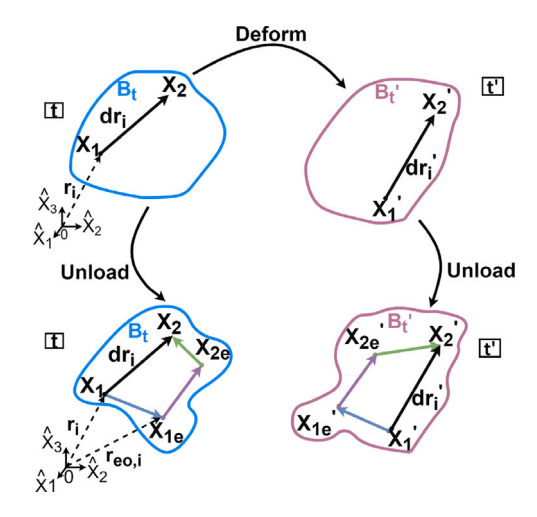


Fig. 2. Displacement of the reconstructed displacement gradient tensor after incorporating traditional definition and experimental observation in continuum motion.

the mathematical derivations at the condition of finite deformations are not the focus of this paper.

We replace the $u_{eo,i}(r_{eo,i}+dr_{eo,i})$ term in Eq. (13) with the truncated form shown in Eq. (14), and we obtain

$$dr'_{eo,i} = dr_{eo,i} + dr_{eo,j} \frac{\partial u_{eo,i}(r_{eo,i})}{\partial r_{eo,i}},$$
(15)

which relates the relative displacement between material equilibrium state, $dr'_{eo,i}$, in the deformed body to the displacement in the undeformed body, $dr_{eo,i}$, through

$$\frac{\partial u_{eo,i}(r_{eo,i})}{\partial r_{eo,j}} = \frac{\partial u_{eo,i}}{\partial x_j}.$$
 (16)

The further simplification, presented as the right-hand side of Eq. (16), is done by realizing the components of x_j constitutes the coordinates of $r_{eo,j}$. The nine components $\frac{\partial u_{eo,j}}{\partial x_j}$ form a second-order tensor, which we call the displacement gradient tensor of the stress-free equilibrium state. The detailed displacement gradient tensor that describes the displacement *from* the stress-free state is derived in the supplementary material, returning the general equation

$$dx_{j}\frac{\partial u_{eo,i}}{\partial x_{i}} + \left[dr'_{ef,i} - dr_{ef,i}\right] = dx_{j}\frac{\partial u_{i}}{\partial x_{i}},\tag{17}$$

after following the simplification done in Eq. (16). The term $\left[dr'_{ef,i} - dr_{ef,i}\right]$ is now written in the form of a displacement gradient tensor, which gives

$$dx_j \frac{\partial u_{eo,i}}{\partial x_j} + dx_j \frac{\partial u_{ef,i}}{\partial x_j} = dx_j \frac{\partial u_i}{\partial x_j}.$$
 (18)

As can be seen in Eq. (18), the traditional displacement gradient tensor $\frac{\partial u_i}{\partial x_j}$, which we refer to as the total displacement gradient tensor, is a sum of the displacement gradient tensor of the equilibrium state $\frac{\partial u_{e_{0,i}}}{\partial x_j}$, and displacement gradient tensor from the equilibrium state $\frac{\partial u_{e_{0,i}}}{\partial x_j}$. The conclusion that the total displacement gradient tensor can be decomposed into two component shapes not only the formalism we use, but also changes our approach to making measurements of viscoelastic material behaviors. It highlights the merits of constructing constitutive models to take the two displacement gradient tensors into consideration. Further, the two displacement gradient tensors imply the existence of two velocity gradient tensors that define two rate of strain tensors and two strain tensors.

The physical interpretations of the two displacement gradient tensors can be explored by considering the Hookean elastic solids and Newtonian viscous fluids cases. For a Newtonian viscous fluid that displays no recovery when loads are removed, the stress-free equilibrium states are always identical to the location of the two material points. That is, the unrecoverable contribution represents the displacement of the equilibrium state. For a Hookean solid whose elasticity allows it to return to its reference configuration after releasing the load, the recoverable contribution is represented by the displacement tensor from the equilibrium state. The strain tensors are then obtained in the normal way by decomposing the three displacement gradient tensors into symmetric and antisymmetric parts as

$$\frac{\partial u_i}{\partial x_j} = \frac{1}{2} \left(\frac{\partial u_i}{\partial x_j} + \frac{\partial u_j}{\partial x_i} \right) + \frac{1}{2} \left(\frac{\partial u_i}{\partial x_j} - \frac{\partial u_j}{\partial x_i} \right), \tag{19}$$

$$\frac{\partial u_{eo,i}}{\partial x_i} = \frac{1}{2} \left(\frac{\partial u_{eo,i}}{\partial x_i} + \frac{\partial u_{eo,j}}{\partial x_i} \right) + \frac{1}{2} \left(\frac{\partial u_{eo,i}}{\partial x_j} - \frac{\partial u_{eo,j}}{\partial x_i} \right), \tag{20}$$

$$\frac{\partial u_{ef,i}}{\partial x_i} = \frac{1}{2} \left(\frac{\partial u_{ef,i}}{\partial x_j} + \frac{\partial u_{ef,j}}{\partial x_i} \right) + \frac{1}{2} \left(\frac{\partial u_{ef,i}}{\partial x_j} - \frac{\partial u_{ef,j}}{\partial x_i} \right). \tag{21}$$

We denote the symmetric part as the displacement gradient of the body free of rotation or translation and is the infinitesimal strain tensor [6]. The three displacement gradient tensors give rise to three strain tensors, which are

$$\gamma_{ij} = \frac{1}{2} \left(\frac{\partial u_i}{\partial x_j} + \frac{\partial u_j}{\partial x_i} \right) = \gamma = \gamma_{tot}, \tag{22}$$

$$\gamma_{eo,ij} = \frac{1}{2} \left(\frac{\partial u_{eo,i}}{\partial x_i} + \frac{\partial u_{eo,j}}{\partial x_i} \right) = \gamma_{unrec}, \tag{23}$$

$$\gamma_{ef,ij} = \frac{1}{2} \left(\frac{\partial u_{ef,i}}{\partial x_i} + \frac{\partial u_{ef,j}}{\partial x_i} \right) = \gamma_{rec}.$$
(24)

Following Eq. (18), we also conclude that

$$\gamma_{tot} = \gamma_{unrec} + \gamma_{rec}. \tag{25}$$

Eq. (25) underlines that the strain, or the total strain, can be decomposed into a sum of recoverable and recoverable contributions. Taking derivatives with respect to time of the three strain tensors allows us to determine the (symmetric) rate of strain tensors as

$$\dot{\gamma}_{ij} = \frac{\mathrm{d}\gamma_{ij}}{\mathrm{d}t} = \frac{1}{2} \left(\frac{\partial v_i}{\partial x_j} + \frac{\partial v_j}{\partial x_i} \right) = \dot{\gamma}_{tot},\tag{26}$$

$$\dot{\gamma}_{eo,ij} = \frac{\mathrm{d}\gamma_{eo,ij}}{\mathrm{d}t} = \frac{1}{2} \left(\frac{\partial v_{eo,i}}{\partial x_j} + \frac{\partial v_{eo,j}}{\partial x_i} \right) = \dot{\gamma}_{unrec},\tag{27}$$

$$\dot{\gamma}_{ef,ij} = \frac{\mathrm{d}\gamma_{ef,ij}}{\mathrm{d}t} = \frac{1}{2} \left(\frac{\partial v_{ef,i}}{\partial x_i} + \frac{\partial v_{ef,j}}{\partial x_i} \right) = \dot{\gamma}_{rec}. \tag{28}$$

Following the rule of linearity, the summation returns

$$\dot{\gamma}_{tot} = \dot{\gamma}_{unrec} + \dot{\gamma}_{rec},\tag{29}$$

where

$$v_i = \dot{u}_i = \frac{\mathrm{d}u_i}{\mathrm{d}t},\tag{30}$$

$$v_{eo,i} = \dot{u}_{eo,i} = \frac{\mathrm{d}u_{eo,i}}{\mathrm{d}t},\tag{31}$$

$$v_{ef,i} = \dot{u}_{ef,i} = \frac{\mathrm{d}u_{ef,i}}{\mathrm{d}t}.$$
 (32)

The total shear rate is therefore the sum of the unrecoverable and recoverable shear rates.

3. Experiments

3.1. Materials

All experiments were performed on surfactant solutions of $3.2~\rm wt~\%$ of cetylpryridinum chloride (CpyCl, Spectrum Chemical) in a $100~\rm mM$ sodium chloride solution (NaCl, Sigma-Aldrich) with a molar ratio

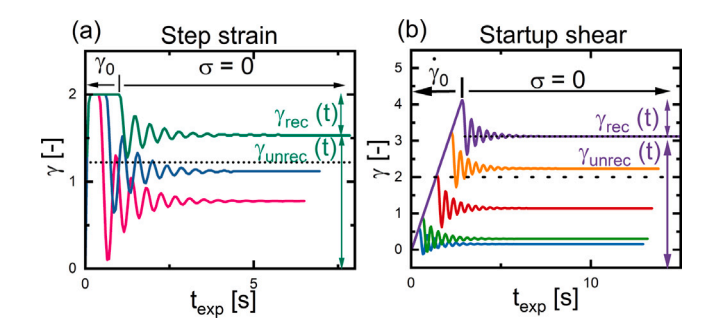


Fig. 3. Demonstrations of iterative (*a*) step strain with recovery and (*b*) startup of steady shear with recovery protocols. In each case, the same initial condition is applied, either as a constant strain or constant strain rate, and the duration of this step is iteratively lengthened, allowing us to map the recoverable and unrecoverable strains as a function of experimental time.

of sodium salicylate (NaSal, Sigma-Aldrich) to CpyCl of 0.5. Such a wormlike micellar (WLM) system falls into the semi-dilute regime [43, 44], making it a model system for studying the reversibly entangled polymeric systems [45–47]. All materials were used as received without further purification. The solution was prepared by firstly adding the required amount of the NaSal into the pre-made NaCl solution followed by CpyCl. All contents were gently mixed and left for at least 48 h before experiments to ensure the solution was homogeneous before performing any rheological measurements.

3.2. Viscoelastic characterizations

Rheological measurements were performed using an Anton Paar Modular Compact Rheometer (MCR) 702 in a single-drive mode. The electrically commutated motors allow measurements under straincontrolled and stress-controlled modes on one device [48]. This device provides a reliable switch between strain-controlled step strain and startup shear and stress-controlled recovery steps within the order of milliseconds. Linear viscoelastic (LVE) spectra of WLM are determined by oscillatory shearing at a small strain amplitude ($\gamma_0 = 0.063$), which is within the moduli-independent regime determined from strain amplitude sweeps. The procedures for performing step strain and startup shear recovery tests are shown in Fig. 3. A given shear strain represented in Fig. 3(a) or a given shear rate shown in Fig. 3(b) is applied to the system, followed after some time by zero shear stress, allowing the material to reach its equilibrium state at a time of interest. To eliminate any inertia effect for the startup shear recovery measurements, we apply a zero-shear rate step ($\dot{\gamma}_0 = 0$) for a short time t = 0.06 s as an intermediate step between the shearing and zero-stress states [22]. The zero-shear rate step shows a negligible effect on material responses. To map out the recoverable and unrecoverable responses throughout the entire experimental period, we iterate the process varying the duration of the experiment each time before going to the zero-stress state. All experiments use a cone and plate geometry with a radius of 50 mm and an angle of 2° with a smooth surface at a temperature of 22 °C. Consistent results and gap distance have been found from all replicates, without slip affecting the measurements. An evaporation hood was applied to minimize solvent evaporation. All rheological properties were collected via Anton Paar's RheoCompass software.

4. Results and discussion

4.1. Characterization results

We present the LVE responses of the WLM in Fig. 4. For angular frequencies, $\omega \leq 10$ rad/s, the response is well characterized by a single-mode Maxwell model with a relaxation time calculated from the crossover frequency $\lambda = 1/\omega_c = 0.71 \pm 0.042$ s, an elastic plateau

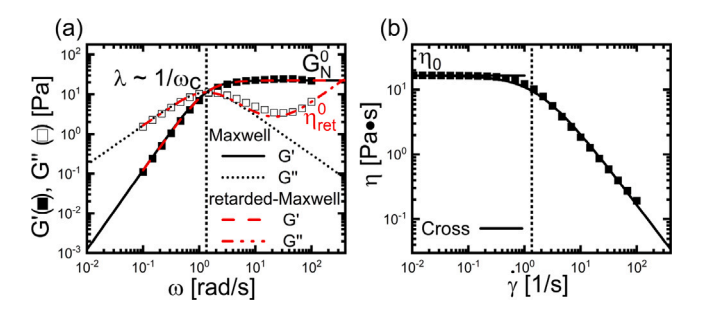


Fig. 4. Viscoelastic characterization of the 3.2 wt% /0.76 wt% CpyCl/NaSal solution at 22 °C (a) frequency-dependent storage (filled symbol) modulus G' and loss (opened symbol) modulus G'' and (b) steady shear flow curve.

Table 1Properties of WLM solution as defined by the linear viscoelastic measurement and steady shear flow curve.

Parameter	Symbol	Value
Relaxation time	λ	$0.71 \pm 0.042 \text{ s}$
Elastic plateau modulus	G_N^0	$23.4 \pm 1.45 \text{ Pa}$
Zero-shear viscosity	η_0	16.6 Pa · s
Retardation viscosity	η_{ret}^0	0.062 Pa · s

modulus $G_N^0 = 23.4 \pm 1.48$ Pa, and a zero-shear viscosity $\eta_0 = \lambda G_N^0 =$ 16.6 Pa · s. Good agreement is found between our data and values reported elsewhere [45]. The zero-shear viscosity obtained from the oscillatory data is consistent with the low-rate plateau value determined from the steady shear characterization as shown in Fig. 4(b). The observation of an upturn in G'' at high frequencies arises from the local Rouse motion or "breathing" of the shortest chains [49]. To capture the upturn, the single-mode Maxwell model can be amended by adding a solvent viscosity η_s . The solvent viscosity is reported to be negligibly small by $\eta_s/\eta_0 = O(10^{-5})$ [50]. We attribute this solvent viscosity to a retardation viscosity η_{ret}^0 as it accounts for the retarding effects at high frequencies. At short timescales or high frequencies under the imposition of small deformation, the network resists rearrangement, including rotation and extension of strands, and the dynamics are dominated by elastic properties [51]. Moreover, as we show later in Section 4.2, the retardation viscosity calculated from the LVE measurement shows quantitative agreement with the retarded dashpot value analyzed from the analytic equation of the Kelvin-Voigt model [52,53]. The numerical values of the characterization values are tabulated in Table 1.

The flow curve obtained from steady shearing at low shear rates exhibits Newtonian behavior characterized by the zero-shear viscosity, which is consistent with the value extrapolated from the oscillatory LVE responses. At shear rates higher than the inverse of the relaxation time, that is, when $\lambda\dot{\gamma}>1$, the system shear-thins, and the steady shearing data can be well described by the inelastic Cross model, as shown in Fig. 4(b) [49]. The Weissenberg number, Wi, is conventionally defined as the product of the relaxation time and shear rate [54,55] and represents a normalized strength of the flow. When $\lambda\dot{\gamma}>1$, the micellar solution shows non-Newtonian behavior.

In Fig. 5, we show the stress relaxation behaviors of the WLM system after being subjected to a series of step strains with a wide range of amplitudes. The underlying assumption of the step strain is that the desirable strain amplitude is applied instantaneously to the material at t=0 [6]. However, due to instrument limitations, the imposed strain amplitude is delayed by 0.2 s before reaching the desirable value and remaining constant as shown in Fig. 5(a). Therefore, all time-resolved results presented in Section 4.2 are collected at times longer than 0.2 s to ensure accuracy of the imposed desirable strain. The time-resolved and strain-dependent relaxation modulus $G(t,\gamma_0)$ is displayed in Fig. 5(b). In the limit of small strain amplitudes ($\gamma_0 \ll 1$), the relaxation modulus is independent of the applied strain, which allows

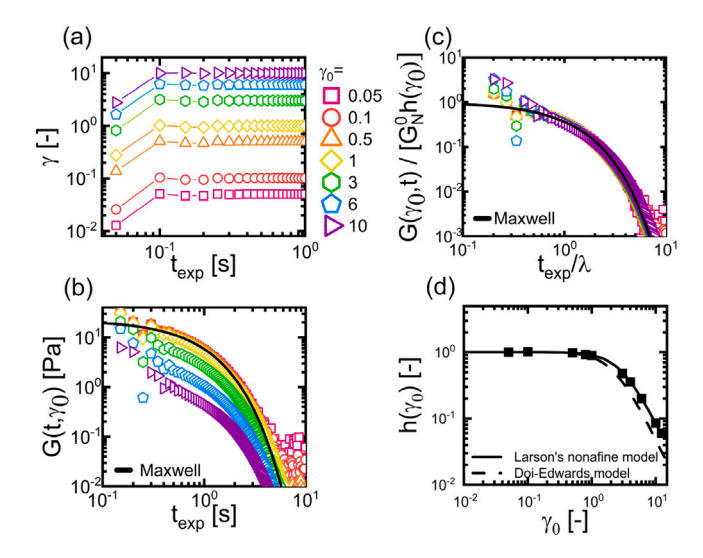


Fig. 5. Stress relaxation as a function of experimental time after applying a wide range of strain amplitudes at t=0 to a material initially at rest state. (a) Strain amplitude γ_0 versus time. (b) Relaxation modulus $G(\gamma_0,t) = \sigma(t,\gamma_0)/\gamma_0$ versus time. (c) Normalized relaxation modulus $G(\gamma_0,t)/[G_\infty h(\gamma_0)]$ versus time, where the damping function is determined as $h(\gamma_0) = G(\gamma_0,t)/G(t)$. (d) The damping function $h(\gamma_0)$ versus applied strain amplitude.

it to be written as $G(t) = \sigma(t)/\gamma_0$. In this small deformation limit, the relaxation modulus decays in a single exponential manner, showing Maxwellian behavior $G(t) = G_N^0 exp(-t/\lambda)$, in which the elastic plateau modulus and the relaxation time are the same as those tabulated in

Once the applied strain amplitudes are within the nonlinear regime $(\gamma_0 > 1)$, the relaxation modulus is time- and strain-dependent, $G(t, \gamma_0) =$ $\sigma(t)/\gamma_0$. At times longer than the relaxation time, all relaxation modulus curves exhibit similar exponential decay, and a vertical shift leads to a superposition of all curves obtained from various amplitudes. The superposition is clearly shown in Fig. 5(c) after scaling the relaxation modulus by the vertical shift factor known as the damping function, $h(\gamma_0)$ [42], with reference curves obtained in the linear viscoelastic limit. For times shorter than the relaxation time, the behavior strongly depends on strain amplitude. The full relaxation mechanisms are well described by the Doi-Edwards tube model as a combination of chain retraction at shorter time and reptation at longer time [8]. Once the experimental time is longer than the retraction time, the relaxation modulus can be factored into time- and strain-dependent terms as $G(t, \gamma_0) = G(t)h(\gamma_0)$, suggesting the principle of time-strain separability. This separability was first identified experimentally in various polymeric systems by Einaga et al. and Osaki et al. [56,57]. The experimental damping function is plotted in Fig. 5(d) as a function of the strain amplitude. The damping function is not as strain-softening as predicted by the Doi-Edwards model. The deviation has previously been explained as an incomplete retraction during reptation. That is, retraction increases the stiffness of the damping function [8]. With the inclusion of partial retraction, Larson's nonaffine model [8] predicts

$$h(\gamma_o) = \frac{1}{1 + \frac{\zeta'}{3}} \gamma_0^2,\tag{33}$$

with a fitted value $\zeta' = 0.33$, close to the values reported elsewhere in the literature for the same system [45].

4.2. Development of constitutive model

After performing the step strain and startup shear recovery measurements in the transient manner as shown in Fig. 3, we calculate the recoverable modulus and flow viscosity, G_{rec} and η_{flow} , using Eqs. (1)–(2). The data obtained from step strain recovery is represented in

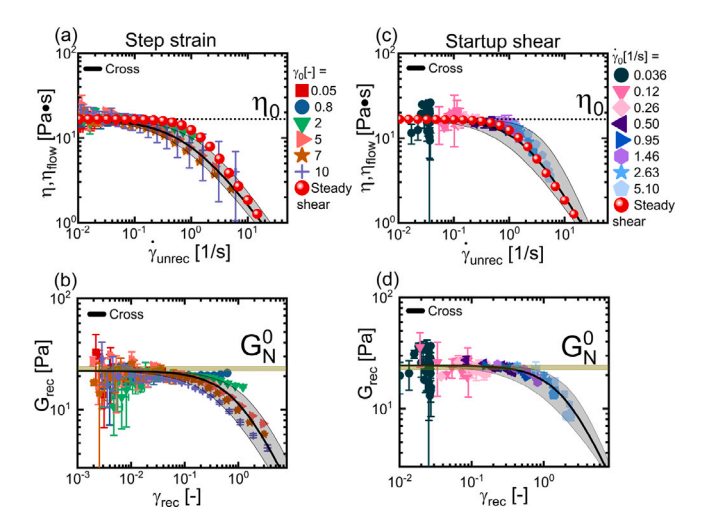


Fig. 6. Time-resolved recovery measurements at 22 °C for recoverable modulus $G_{rec}(t) = \sigma(t, \gamma_0)/\gamma_{rec}(t)$ and flow viscosity $\eta_{flow}(t) = \sigma(t, \gamma_0)/\gamma_{unrec}(t)$ determined from (a)—(b) step strain recovery and (c)—(d) startup shear recovery tests. Dark yellow regions between dotted lines represent the standard deviation of the elastic modulus G_N^0 obtained from linear viscoelastic measurements. A gray area is used as a visual aid for showing which portions of data are used for fitting analysis.

Figs. 6(a)-(b) and the data collected from the startup shear recovery is shown in Figs. 6(c)-(d). Similar test protocols were performed in [22] at only one linear strain amplitude and two strain rates. In this paper, we performed the two test protocols at a wide range of shear strains and rates in both linear and nonlinear regimes to investigate the material's responses fully. We show the time-resolved recoverable modulus and flow viscosity as functions of the recoverable strain and unrecoverable rate. Viscous flow is represented by the flow viscosity and elastic deformations are described by the recoverable modulus. The large error bars found at small recoverable strains ($\gamma_{rec} \sim O(10^{-3})$) and unrecoverable shear rates ($\gamma_{unrec}^{\cdot \cdot} \sim O(10^{-2})$) arise from dividing two small values. The linear material properties are labeled to compare with the recovery material functions obtained at small recoverable strains and unrecoverable shear rates. The steady shear flow curve is also shown in Figs. 6(a) and 6(c) to serve as a comparison. In the step strain tests, the largest unrecoverable rates and recoverable strains correspond to the earliest times of the test.

As can be seen from Figs. 6(a) and 6(c), the unrecoverable flow behavior observed in step strain experiments at different strain amplitudes and steady shear start-up at different shear rates matches the behavior of the steady state flow curve. That is, there is a direct and remarkable equivalence between the response to step strain behavior and the steady state flow curve. In the traditional analyzes that are based on the total strain and total rate, the transient stress observed in a step-strain test is said to be due to an evolving (Hookean) elastic modulus, $\sigma(t) = G(t)\gamma_0$. Similarly, in a steady shear start-up experiment, the transient stress is said to be due to an evolving (Newtonian) viscosity, $\sigma(t) = \eta^+(t)\dot{\gamma}$. This underlying assumption has led to the development of a constitutive model for analyzing small and large amplitude oscillatory shear [58]. Responses from the two test protocols are therefore difficult to compare as the common metrics associated with each test have different units. The assumption that all transience is tied to either a modulus or a viscosity, and not both, neglects the simultaneous contributions of recoverable strains and unrecoverable rates. When viewed from an ylikócentric perspective in terms of the recovery metrics implied by the formalism presented in Section 2, it becomes clear that transient stress responses can be caused by both elastic and viscous effects, allowing for direct comparison across different deformation protocols. The clear comparison between the tests we present in Fig. 6 can be explained simply by noting that the viscous curves shown in (a) and (c) represent

Table 2 Modeling parameters for recoverable modulus G_{rec} and flow viscosity η_{flow} obtained for the WLM under step strain and startup shear recovery measurements

Parameter	Symbol	Value
η_{flow} Cross model prefactor	а	0.83 ± 0.5
η_{flow} Cross model power index	b	1.02 ± 0.165
G_{rec} Cross model prefactor	c	0.71 ± 0.44
G_{rec} Cross model power index	d	1.31 ± 0.35

the unrecoverable contributions alone, while the elastic curves shown in (b) and (d) represent the recoverable contributions.

The similarities between the trends depicted by recovery material functions and recovery measurements are obvious, even though the two test protocols are drastically different. What we can see from both tests is that the WLM solution displays both (recoverable) strain-softening and (unrecoverable) shear-thinning. That is, the recoverable modulus decreases with increasing recoverable strain and the flow viscosity decreases with increasing unrecoverable shear rate. At small recoverable strains and unrecoverable shear rates, the recoverable modulus and flow viscosity are equal to the plateau modulus and the zeroshear viscosity for the two protocols, indicating the close proximity to equilibrium. The step strain protocol applies a theoretically discontinuous but practically continuous deformation to the material and allows the material to relax. The deformation therefore switches from being recoverable to unrecoverable. In contrast, the startup shear applies continuous deformation to the material. Regardless of the different types of deformation applied in the step strain and startup shear recovery tests, we determine uniform behavior from an ylikócentric perspective.

The material behavior in terms of the recoverable modulus and flow viscosity are well described by Cross-type functions [59]. To represent the shear-thinning flow viscosity, we replace the total shear rate, $\dot{\gamma}_0$, by the unrecoverable shear rate, $\dot{\gamma}_{unrec}$,

$$\eta_{flow}(\dot{\gamma}_{unrec}) = \frac{\eta_0}{1 + (a\dot{\gamma}_{unrec})^b}.$$
 (34)

The parameters a and b in Eq. (34) are material properties. The parameter a implies the degree of shear dependence on the structural breakdown, and b is the flow index. To describe the strain-softening behavior of the recoverable modulus, we again make use of the Cross model, but replace the unrecoverable shear rate, $\dot{\gamma}_{unrec}$, with the recoverable strain, γ_{rec} , and the zero-shear viscosity by the plateau modulus,

$$G_{rec}(\gamma_{rec}) = \frac{G_N^0}{1 + (c\gamma_{rec})^d}.$$
 (35)

Here, the parameters c and d take on similar interpretations to a and b in Eq. (34). A similar strain-dependent model was proposed for cohesive suspensions [60], but with a reliance on the total strain rather than the recoverable strain that is our focus here. As shown in Fig. 6, the (unrecoverable) shear-thinning and (recoverable) strain-softening descriptions, presented by the thick solid lines, match the recovery material functions well. The agreement implies the applicability of the descriptions is insensitive to the type of deformation. The numerical values of the model parameters used for generating the fits are identical within the standard deviations and are shown in Table 2.

To make the most of our experimental data, we also pay attention to the creep ringing response during the recovery steps, which was not studied in [22] and is a result of a coupling between the elasticity and the inertia of the system. The observation of a decaying envelope clearly indicates that using the shear-thinning and strain-softening contributions, as displayed in Eqs. (34) and (35), will be insufficient to provide complete interpretations for all the behaviors observed. An additional viscous term is needed to account for the decaying oscillations. We use the ringing solution for a Kelvin–Voigt element [52,53] to analyze the zero-stress recovery step to calculate the

retardation viscosity η_{ret} . The solution written in terms of parameters defined in recovery rheology is

$$\gamma(t_{rec}) = \gamma_{rec} \times \left[1 - e^{-A_{rec}t_{rec}} \left[\cos(\omega_{rec}t_{rec}) + \frac{A_{rec}}{\omega_{rec}} \sin(\omega_{rec}t_{rec}) \right] \right].$$
(36)

In Eq. (36), t_{rec} is the recovery time, $\gamma_{rec} = \frac{\sigma}{G_{rec}}$, $A_{rec} = \frac{\eta_{ret}b_{geo}}{2I}$, and $\omega_{rec} = \sqrt{\frac{G_{rec}b_{geo}}{I} - A_{rec}^2}$. I represents the sum of the geometry and instrument inertia returned by the calibration protocol performed by the RheoCompass software, and b_{geo} is a geometry factor that for a cone-and-plate geometry with cone angle θ is $2\pi R^3/3\tan(\theta)$. Eq. (36) is further rearranged to

$$1 - \frac{\gamma(t_{rec})}{\gamma_{rec}} = e^{-A_{rec}t_{rec}} \left[\cos(\omega_{rec}t_{rec}) + \frac{A_{rec}}{\omega_{rec}} \sin(\omega_{rec}t_{rec}) \right]$$
 (37)

to allow for easier extraction of the retardation viscosity directly from the slope A_k after performing the linear regression in a semilog plot.

The resultant retardation viscosity as a function of recovery time found from step strain recovery and startup shear recovery test is shown in Figs. 7(a) and 7(b), respectively. A constant value is found across a range of strain amplitudes and shear rates tested. The retardation viscosity obtained from step strain recovery η_{ret}^{step} is 0.058 Pa·s and the one collected from startup shear recovery $\eta_{ret}^{startup}$ is 0.081 Pa·s. The retardation viscosity extracted from analyzing the creep-ringing phenomenon is nearly identical to the retardation viscosity found from fitting the high frequency responses of the loss modulus in the LVE frequency sweep. We attribute the small differences to batch-to-batch variations in sample concentrations. Aside from allowing us to determine the retardation viscosity for the two recovery measurements, the creep ringing response proves the Cross-type function for the strain softening recoverable modulus we proposed in Eq. (35). The oscillatory parts collected from the step strain and startup recovery are represented in Figs. 7(c) and 7(d). The waveforms are both frequency- and amplitudemodulated, especially for the larger step strain tests. As the recoverable strain decreases, the frequency increases and the oscillation recovers to its equilibrium value seen in the linear regime. Since frequency is directly proportional to the recoverable modulus as shown in Eq. (36), a similar relationship exists between the recoverable strain and the recoverable modulus, precisely captured in Figs. 6(b) and 6(d).

The ylikócentric observations afforded by our recovery rheology protocols in the linear and nonlinear regimes lead us to the development of a new constitutive model. Our model is similar to the retarded-Maxwell model, which has provided molecular interpretations of polymeric systems undergoing deformations [51]. Our model captures linear as well as nonlinear responses by incorporating the nonlinear elastic and viscous functions shown in Eqs. (34) and (35). The complete formalism of our model is

$$\eta_{flow}\left(\dot{\gamma}_{0} \cdot \frac{1 + c\gamma_{rec}^{d} - cd\gamma_{rec}^{d}}{1 + c\gamma_{rec}^{d}} + \frac{\eta_{ret}}{G_{rec}} \dot{\gamma}_{0}\right) = \dot{\sigma} \frac{\eta_{flow} + \eta_{ret}}{G_{rec}} + \sigma \left(\frac{1 + c\gamma_{rec}^{d} - cd\gamma_{rec}^{d}}{1 + c\gamma_{rec}^{d}} - \frac{\eta_{ret}}{G_{rec}} \frac{ab\ddot{\gamma}_{unrec}\dot{\gamma}_{unrec}^{b-1}}{1 + a\dot{\gamma}_{unrec}^{b}}\right).$$
(38)

Previous efforts have introduced only one nonlinear element to generate complex behavior. For example, the White–Metzner model [61] replaces the constant viscosity with a nonlinear function that depends on the second invariant of the deformation tensor. Nonlinear elastic behaviors have also been used and are well discussed in terms of the finite extensible elastic (FENE) model [62]. Few studies have created models that consist of both nonlinear elastic and viscous terms to replicate the creep and stress relation of polymeric solutions [63,64].

The predictions of the model are compared with the time-resolved material responses in Fig. 8. Derivations of the model expressions used can be found in the supplementary material. The comparisons for step strain recovery measurements are shown in Figs. 8(a)–(c), and for

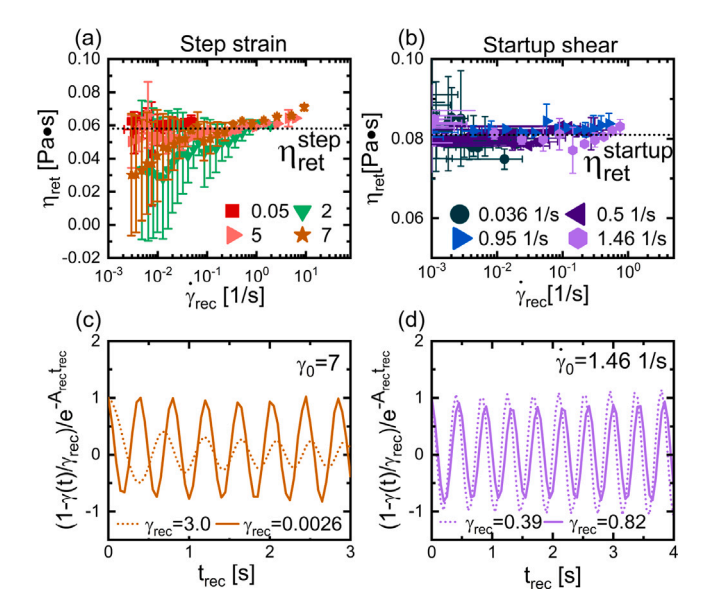


Fig. 7. Retardation viscosity obtained for step strain in (a) and (c) and startup shear in (b) and (d) recovery tests for strain amplitudes and shear rates ranging from linear to nonlinear regimes. Comparison of waveforms at two different experiment times for the highest strain amplitude (c) and strain rate (d).

the startup shear recovery measurements, the results are compared in Figs. 8(d)–(f). Even though the magnitudes of the nonlinear strain amplitude differ by a factor of 5, the maximum recoverable strains achieved at the earliest times only differ by a factor of about 2, as can be found in Fig. 8(b). The small difference suggests that elastic energy stored in the stretched WLM strands has an upper limit. Similar phenomena are observed in the startup shear experiments, in which all strain is recoverable at the earliest time, and the unrecoverable strain dominates the long-time behavior, as represented in Figs. 8(e) and 8(f).

The predictions of our model show excellent agreement with the experimental data for the step strain recovery scenario, even at the largest nonlinear strain amplitude of $\gamma_0=7$. For the startup shear, the model captures the nonlinear responses well up to shear rate of 2.63 1/s. The model does not predict stress overshoots and so deviates from the experimental data when the shear rate exceeds $\dot{\gamma}=2.63$ 1/s. Higher shear rates $\dot{\gamma}\gg 2.63$ 1/s, are not explored due to the complexity from the presence of shear-banding [46]. Despite its simplicity, our model provides accurate predictions of nonlinear rheological data collected from different types of deformations, including very large step strains.

One of the benefits of recovery rheology allowing for transient material parameters is the ability to clearly identify the governing physics. In the case of the WLMs studied here, it is well known that in the fast-breaking limit they behave as an entangled polymeric system with uniform molecular weight. As in polymeric network theory, the plateau modulus provides insight into the molecular weight between entanglements, and therefore how tightly knitted the network is. We have already established an equivalence between the recoverable and plateau moduli and now look to how the entanglement of the network is affected by the shear protocols we have investigated here.

The transient entanglement length $l_{e,l}$, representing a chain length between two entanglements, allows us insight into the influence of deformations on the microstructure of the WLM network. Under the assumptions of good solvent conditions, and making the mean-field approximation [43], the entanglement length l_e is [41]

$$l_e \sim \zeta^{5/3} b^{-2/3}$$
. (39)

In Eq. (39), the correlation length ζ is calculated from the relation $\zeta \sim (k_b T/G_N^0)^{1/3}$, in which G_N^0 is the elastic plateau modulus, and b

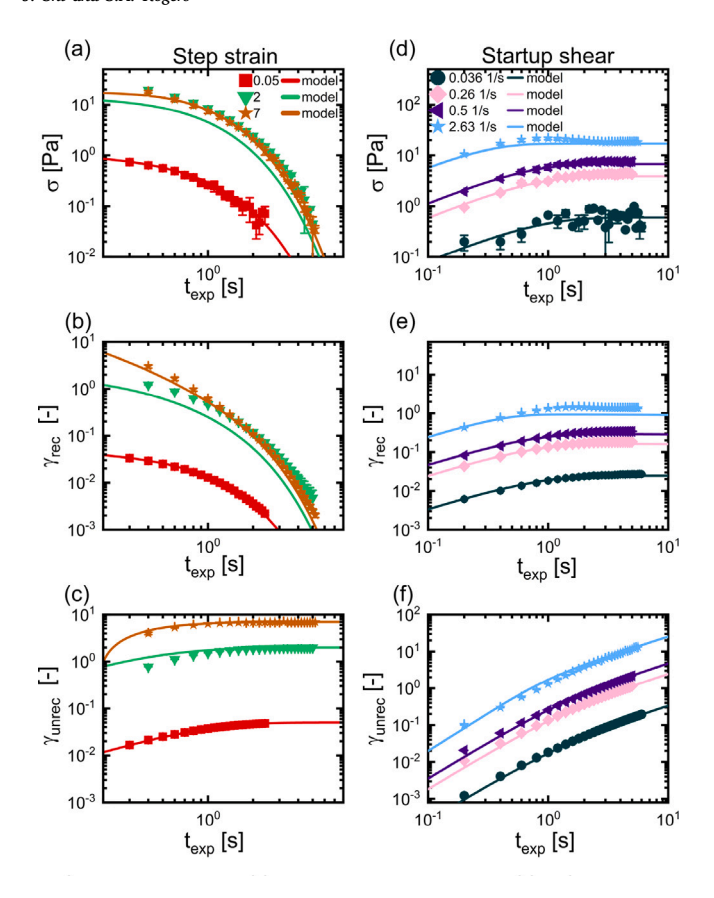


Fig. 8. Recoverable strain γ_{rec} , unrecoverable shear rate $\dot{\gamma}_{unrec}$, and shear stress σ versus experimental time t_{exp} for step strain (a)–(c) and startup shear (d)–(f) recovery tests.

is the persistence length of the WLM, which is typically assumed to be 15 nm for CPy/Sal [43]. To determine how the entanglement length changes during experimental times, we revise Eq. (39) by replacing the constant elastic plateau modulus by the time-varying recoverable modulus, $\zeta \sim (k_b T/G_{rec})^{1/3}$. The data of the transient entanglement length as a function of experimental time is shown in Fig. 9. In step strain experiments, the temporal network is initially perturbed elastically. The network then adjusts to the new condition as time progresses. If the imposed strain amplitude is within the linear region ($\gamma_0 \le 1$), the network is weakly perturbed, and the transient entanglement length remains constant. For large strain amplitudes ($\gamma_0 \ge 1$), the network experiences enforced topological changes and the transient entanglement length is expected to increase. In such a case, the transient entanglement length will be inversely proportional to time since the step, as seen in Fig. 9(a). The transient entanglement length is plotted as a function of recoverable strain in Fig. 9(c). In a similar manner to non-Newtonian flow behavior occurring at rates in excess of 1/a from Eq. (34), the topological changes, as shown by the deviation of the equilibrium entanglement length found at the lower limit, occur at recoverable strains around 1/c determined from the recoverable modulus, as shown in Eq. (35).

In the case of startup shear, if the shear rate imposed is large (Wi >1), the response will deviate from linearity, and WLM strands are gradually moved apart. The idea is supported by the data of Fig. 9(b) in which the transient entanglement length is shown to increase with increased straining. Similar behavior is found when plotting the transient entanglement length as a function of recoverable strain as shown in Fig. 9(d). The steady-state value of the transient entanglement length at small shear rates and small step strains is calculated to be 0.14 μm , close to the literature value $l_{e,lit}$ ($\sim 0.13~\mu m$) reported for similar concentration of the same WLM system [45].

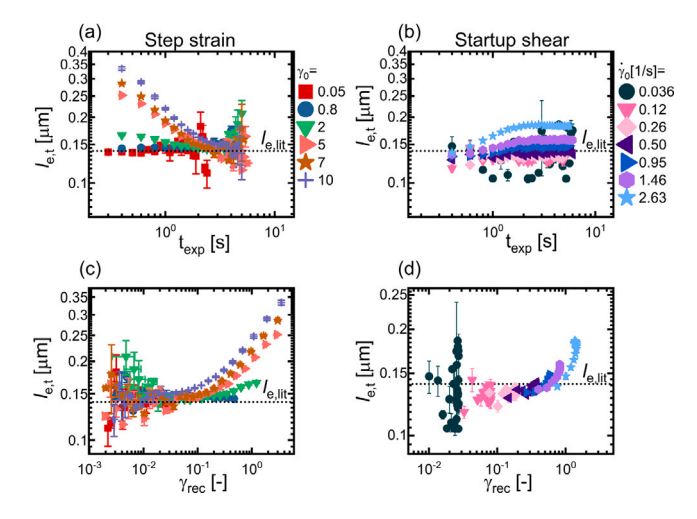


Fig. 9. Transient entanglement length $l_{e,t}$ versus experimental time t_{exp} for (a) step strain and (b) startup shear, and transient entanglement length $l_{e,t}$ versus recoverable strain γ_{rec} obtained for (c) step strain and (d) startup shear recovery tests in wide range of strain amplitudes γ_0 and shear rates $\dot{\gamma}$.

4.3. Discussions of material properties

The first material property we will discuss is the relaxation time [2, 5]. The recovery rheology metrics and the construction of our model lead us to define an instantaneous relaxation time as

$$\lambda_{rec}(t) = \frac{\eta_{flow}(t) + \eta_{ret}(t)}{G_{rec}(t)} \approx \frac{\eta_{flow}(t)}{G_{rec}(t)}. \tag{40}$$

Because of the small value of the retardation viscosity found from analyzing the creep-ringing response, we can neglect it and simplify the relaxation time to be the ratio of the flow viscosity to the recoverable modulus. As has been discussed previously, the temporal network formed by the WLM strands disentangles when large strains or shear rates are applied. For large step strains, WLM strands are disentangled by the large strain and then re-entangle as a function of experimental time. For startup of steady shear, WLM strands disentangle as more strain is applied over time. Therefore, there is a need to account for the dynamic changes in timescale with respect to the transient configuration. Since the flow viscosity and the recoverable modulus are ratios of the same total stress to the unrecoverable shear rate and the recoverable strain, Eq. (40) can be rewritten completely in terms of measured deformation metrics as [22,55,65]

$$\lambda_{rec} \approx \frac{\eta_{flow}}{G_{rec}} = \frac{\gamma_{rec}}{\dot{\gamma}_{unrec}}.$$
 (41)

The recovery rheology relaxation time shown in Eq. (41) is the same as the one that White defined when introducing the Weissenberg number for the first time [55]. From analysis of the equation of motion for a second-order fluid, White noted the presence of a dimensionless group he called the Weissenberg number,

$$Wi = J_e \omega_1 U / L, \tag{42}$$

where J_e is the steady state compliance, $\omega_1 = \int_0^\infty G(s)ds = \eta_0$ is the zero-shear viscosity, and U and L are a characteristic velocity and length. Recalling that $J_e = \gamma_{rec}/\sigma$ is the inverse of the recoverable modulus defined in Eq. (1), $\omega_1 = \eta_0 = \sigma/\dot{\gamma} = \sigma/\dot{\gamma}_{unrec}$ in the limit $\dot{\gamma} \to 0$, and that U/L is an unrecoverable strain rate, provides for some illuminating simplifications. If we take the common interpretation that the Weissenberg number is the product of a relaxation time and a shear rate, $Wi = \lambda \dot{\gamma}$, then $\lambda = J_e \eta_0 = (\gamma_{rec}/\sigma) \times (\sigma/\dot{\gamma}_{unrec}) = \gamma_{rec}/\dot{\gamma}_{unrec}$ as presented in Eq. (41). One further simplification, that $U/L = \dot{\gamma}_{unrec}$ shows that the Weissenberg number is the recoverable strain, Wi = 0

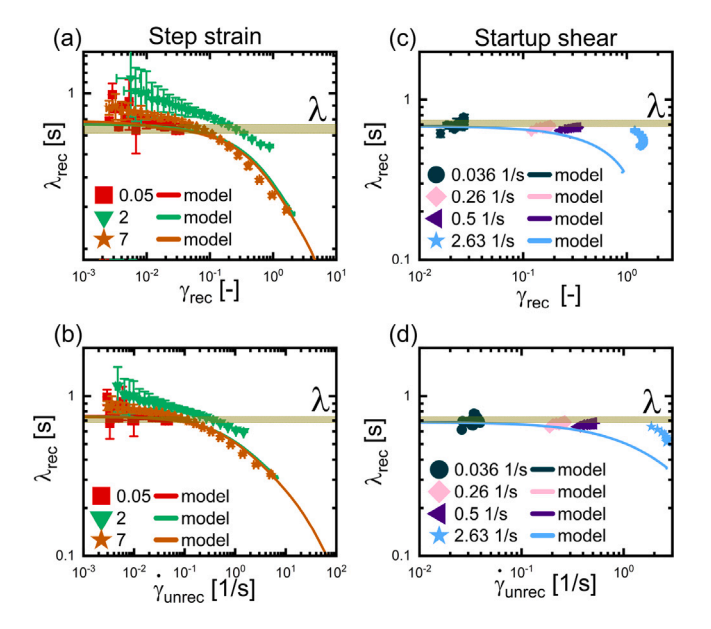


Fig. 10. Instantaneous recovery rheology relaxation time λ_{rec} versus experimental time t_{exp} for step strain (a)–(b) and startup shear recovery tests (c)–(d). The dark yellow region between dotted lines represents the standard deviations of the relaxation time obtained from the linear viscoelastic measurements.

 $\lambda \dot{\gamma} = (\gamma_{rec}/\dot{\gamma}_{unrec}) \times \dot{\gamma}_{unrec} = \gamma_{rec}$. Recovery rheology and the ylikócentric perspective are therefore central to rheological formalisms.

The relationships between the recovery rheology relaxation time and recoverable strain and unrecoverable shear rate are shown in Fig. 10 for the two recovery measurements, along with the model predictions.

It is apparent from the data in Fig. 10 that for both step strain and startup shear measurements, the recovery rheology relaxation time decreases with increasing recoverable strain and unrecoverable shear rate, resembling both the experimental data and the Cross-type behaviors built into the model. This simple model shows that relaxation occurs faster in the nonlinear regime than in the linear regime. Assuming a constant relaxation time to calculate a Weissenberg or Deborah number (where the Deborah number nondimensionalizes the experimental time, $De = \lambda/t_{exp}$) may therefore not describe experimental data well, as soft systems may exhibit faster relaxation rates further from equilibrium, as shown here.

The ideas of recovery rheology are also important to consider in the definition of the damping function. As discussed in Section 4.1, the damping function, $h(\gamma_0)$, is usually defined as the ratio of the nonlinear relaxation modulus, $G(t,\gamma_0)$, to the linear version, G(t). The decaying trend of the damping function in the limit of large strain amplitudes is typically interpreted in terms of the destruction of the network. In general, the damping function, $h(\gamma_0,t)$, is strain- and time-dependent, even though it is defined initially to obey the principle of time-strain separability. Investigations of the time-dependent form have been summarized by Rolón-Garrido and Wagner [66].

To rewrite the damping function based on the idea of recovery rheology, we use the fraction of the recoverable strain in the total strain amplitude. The new definition follows the physical meaning suggested by Wagner and Meissner as the survival probability of the network [42], which is represented as Eq. (43),

$$h_{new} = h(\gamma_0, t_{exp}) = \frac{\gamma_{rec}(t_{exp}, \gamma_0)}{\gamma_0}.$$
(43)

As the new damping function approaches unity, when the recoverable strain is identical to the applied strain amplitude, the elastic energy of the system remains unchanged, and the network is barely perturbed. At the other extreme, when the new damping function

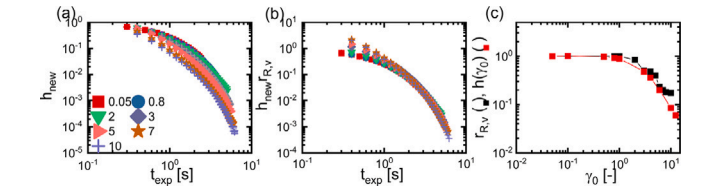


Fig. 11. (a) New damping function h_{new} versus experimental time t_{exp} . (b) Reduced new damping function versus time in which reduced factor $r_{R,V}$ is determined with $r_{R,V} = [h_{new}(\lambda_0, t_{exp})/h_{new}(t_{exp})]$. (c) Reduced factor $r_{R,V}$ and traditional damping function $h(\gamma_0)$ versus strain amplitudes.

approaches zero, the majority of the strain applied is unrecoverable, implying that the network has been destroyed under large straining. When the system undergoes large deformation, the elasticity of the network decreases due to disentanglement. This definition of the damping function directly accounts for the unrecoverable contribution. Because recoverable strain varies with time, this damping function depends on both time and strain amplitude. A similar finding was previously reported that the modulus evolved in the re-entanglement process, showing consistent behavior without the need to invoke the damping function. This result implies the damping function is not required to account for decreases in elasticity [21].

We show in Fig. 11 the new damping function, h_{new} , at strain amplitudes imposed in the step strain experiments. All new damping function curves collected at small strain amplitudes exhibit the same decaying trends. Once the strain amplitude is large enough to elicit nonlinear responses, the new damping function is time- and strain-dependent, as shown in Fig. 11(a). The new damping function shows identical behaviors to the traditional nonlinear relaxation modulus. If we borrow the same idea of determining the conventional damping function, we end up with a superposition of all curves at longer experimental time after applying a vertical shift factor, $r_{R,V}$. In Fig. 11(b), the time-dependent behavior at longer experimental time and the strain-dependent response, represented by the different decreasing slopes at shorter experimental time, follow the principle of time-strain separability. However, the new damping function varies in time as well. It is instructive to compare the resultant vertical shift factor with the traditional damping function, which is also a vertical shift factor, and the comparison is shown in Fig. 11(c). Both qualitative and quantitative similarities are observed between the vertical shift factor and traditional damping function. The pioneering work of Einaga investigated a similar comparison in shift factor determined from the relaxation modulus and recoverable strain [56] without introducing the concept of damping function. Instead, Einaga's work has set forth the experimental validation of the principle of time-strain separability. The time-dependent property enforces the new damping function to deviate from the original definition of the principle. Moreover, the consideration of recoverable strain provides us with opportunities to define transient damping functions for other tests, such as the startup shear. The transient damping function obtained from the startup shear measurement is shown in the supplementary material. Distinct timeand strain-dependent regions can be seen after vertically shifting all the curves with reference to the linear transient damping function.

5. Conclusions

We have explored the implications of a formalism that acknowledges the phenomenon of recovery from a theoretical, experimental, and modeling perspective. This formalism acknowledges the existence of recoverable strain for the displacement gradient tensor and ultimately for the formal definitions of strain and strain rate. The assumption that any past state chosen by the experimenter can be taken as a reference state, what we refer to as the *anthropocentric* view, is true only for generalized Newtonian fluids that display no recovery when

forces are removed. By giving primacy to the material equilibrium state, taking the material-centric or *ylikócentric* view, we are led to the definition of two distinct strains, and two distinct strain rates. This acknowledgment allows us to revise the concept of the displacement gradient tensor, and we show that the traditional measure is composite and can be decomposed into two tensors related to the displacement *from* the equilibrium state and displacement *of* the equilibrium state. The physical meanings for each of the newly derived displacement gradient tensors are directly linked to the recoverable and unrecoverable contributions. The traditional definitions of strains and strain rates are therefore shown to be sums of recoverable and unrecoverable components, $\gamma(t) = \gamma_{rec}(t) + \gamma_{unrec}(t)$, $\dot{\gamma} = \dot{\gamma}_{rec}(t) + \dot{\gamma}_{unrec}(t)$.

The new formalism highlights the need for recovery measurements, which we perform for a range of different shear protocols. The recovery rheology results naturally lead to the development of a new constitutive model that contains nonlinear functions for describing elasticity and viscosity. We performed step strain and startup shear recovery on the CpyCl/NaSal WLM system at various strains and shear rates within the linear and nonlinear regions. The recovery material functions - the recoverable modulus and flow viscosity - were investigated, and Crosstype relations were proposed to characterize the material responses. The retardation viscosity was calculated from the creep-ringing solution of the Kelvin-Voigt element. Despite being based on measures that represent the decomposition of the total strain and rate at infinitesimal deformations, the model shows excellent quantitative agreement with experimental data even for the very largest step strain tests. The favorable predictions support the idea that the decomposition is also applicable for finite deformations.

Definitions of instantaneous relaxation times and damping functions are presented in the framework of recovery rheology. The relaxation time is well approximated by the ratio of the flow viscosity to the recoverable modulus, due to the small value of retardation viscosity. The instantaneous relaxation time is shown to be dependent on both recoverable strain and unrecoverable shear rate. Defining the damping function in terms of the recoverable strain suggests the possibility of determining damping functions in other types of deformation beyond the traditionally used step strain experiments. Characterization of network dynamics to experimental protocols other than step strain tests can therefore be carried out in a consistent manner with the new functions. These findings, and the general principles of recovery rheology provide an enticing avenue to pursue to more deeply understand material responses under nonlinear deformations.

Declaration of competing interest

The authors declare the following financial interests/personal relationships which may be considered as potential competing interests: Simon Rogers reports financial support was provided by American Chemical Society Petroleum Research Fund. Simon Rogers reports financial support was provided by National Science Foundation.

Data availability

Data will be made available on request.

Acknowledgments

We acknowledge the Donors of the American Chemical Society Petroleum Research Fund, United States for support (or partial support) of this research. This work was also supported by the National Science Foundation, United States under the DMREF Award Number DMR-2119172. The authors thank Anton Paar for their support through their VIP academic program.

Appendix A. Supplementary data

Supplementary material related to this article can be found online at https://doi.org/10.1016/j.jnnfm.2023.105113.

References

- R.G. Larson, The Structure and Rheology of Complex Fluids, vol. 150, Oxford university press New York, 1999.
- [2] J.D. Ferry, Viscoelastic Properties of Polymers, John Wiley & Sons, 1980.
- [3] G. Astarita, G. Marrucci, Principles of Non-Newtonian Fluid Mechanics, McGraw-Hill, 1974.
- [4] C.W. Macosko, Rheology principles, in: Measurements and Applications, VCH Publishes, 1994.
- [5] R.B. Bird, R.C. Armstrong, O. Hassager, Dynamics of Polymeric Liquids, vol. 1: Fluid Mechanics. John Wiley and Sons Inc., New York, NY, 1987.
- [6] N.W. Tschoegl, The Phenomenological Theory of Linear Viscoelastic Behavior: An Introduction, Springer Science & Business Media, 2012.
- [7] W. Noll, The Foundations of Mechanics and Thermodynamics: Selected Papers, Springer Science & Business Media, 2012.
- [8] R.G. Larson, Constitutive Equations for Polymer Melts and Solutions: Butterworths Series in Chemical Engineering, Butterworth-Heinemann, 2013.
- [9] J.M. Dealy, K.F. Wissbrun, Melt Rheology and Its Role in Plastics Processing: Theory and Applications, Springer Science & Business Media, 2012.
- [10] X. Oliver Olivella, C. Agelet de Saracibar Bosch, Continuum Mechanics for Engineers. Theory and Problems, 2017.
- [11] C. Truesdell, The mechanical foundations of elasticity and fluid dynamics, J. Ration. Mech. Anal. 1 (1952) 125–300.
- [12] M. Mooney, Secondary stresses in viscoelastic flow, J. Colloid Sci. 6 (1951) 96–107.
- [13] J. Benbow, E. Howells, Normal stress, shear recovery and viscosity in polydimethyl siloxanes, Polymer 2 (1961) 429–436.
- [14] M. Wagner, H. Laun, Nonlinear shear creep and constrained elastic recovery of a LDPE melt, Rheol. Acta 17 (1978) 138–148.
- [15] A.S. Lodge, A network theory of constrained elastic recovery in concentrated polymer solutions, Rheol. Acta 1 (1958) 158–163.
- [16] A.S. Lodge, Elastic Liquids: An Introductory Vector Treatment of Finite-Strain Polymer Rheology, Academic Press, 1964.
- [17] K. Weissenberg, A continuum theory of rhelogical phenomena, Nature 159 (1947) 310–311.
- [18] W. Philippoff, F.H. Gaskins, J.G. Brodnyan, Flow birefringence and stress. V. Correlation of recoverable shear strains with other rheological properties of polymer solutions, J. Appl. Phys. 28 (1957) 1118–1123.
- [19] M. Reiner, Rheology, in: Elasticity and Plasticity/Elastizität und Plastizität, Springer, 1958, pp. 434–550.
- [20] J. Oldroyd, Deformation and flow, Nature (1972) 310-311.
- [21] J.C.-W. Lee, L. Porcar, S.A. Rogers, Recovery rheology via rheo-SANS: Application to step strains under out-of-equilibrium conditions, AIChE J. 65 (2019) e16797.
- [22] P.K. Singh, J.C.-W. Lee, K.A. Patankar, S.A. Rogers, Revisiting the basis of transient rheological material functions: Insights from recoverable strain measurements, J. Rheol. 65 (2021) 129–144.
- [23] J.C.-W. Lee, Y.-T. Hong, K.M. Weigandt, E.G. Kelley, H. Kong, S.A. Rogers, Strain shifts under stress-controlled oscillatory shearing in theoretical, experimental, and structural perspectives: Application to probing zero-shear viscosity, J. Rheol. 63 (2019) 863–881.
- [24] G.J. Donley, P.K. Singh, A. Shetty, S.A. Rogers, Elucidating the g overshoot in soft materials with a yield transition via a time-resolved experimental strain decomposition, Proc. Natl. Acad. Sci. 117 (2020) 21945–21952.
- [25] K. Kamani, G.J. Donley, S.A. Rogers, Unification of the rheological physics of yield stress fluids, Phys. Rev. Lett. 126 (2021) 218002.
- [26] G.J. Donley, J.R. de Bruyn, G.H. McKinley, S.A. Rogers, Time-resolved dynamics of the yielding transition in soft materials, J. Non-Newton. Fluid Mech. 264 (2019) 117-134
- [27] J. Choi, M. Armstrong, S.A. Rogers, The role of elasticity in thixotropy: Transient elastic stress during stepwise reduction in shear rate, Phys. Fluids 33 (2021) 033112
- [28] J.G. Oldroyd, A rational formulation of the equations of plastic flow for a Bingham solid, Math. Proc. Camb. Phil. Soc. 43 (1947) 100-105.
- [29] K. Hashiguchi, Nonlinear Continuum Mechanics for Finite Elasticity-Plasticity: Multiplicative Decomposition with Subloading Surface Model, Elsevier, 2020.
- [30] E. Kröner, Kontinuumstheorie Der Versetzungen Und Eigenspannungen, vol. 5, Springer, 1958.
- [31] E.H. Lee, Elastic-plastic deformation at finite strains, 1969.
- [32] C.J. Dimitriou, G.H. McKinley, A canonical framework for modeling elastoviscoplasticity in complex fluids, J. Non-Newton. Fluid Mech. 265 (2019) 116–132.
- [33] M.E. Gurtin, E. Fried, L. Anand, The Mechanics and Thermodynamics of Continua, Cambridge University Press, 2010.

- [34] K.R. Rajagopal, A.R. Srinivasa, A thermodynamic frame work for rate type fluid models, J. Non-Newton. Fluid Mech. 88 (2000) 207–227.
- [35] K. Rajagopal, A. Srinivasa, Modeling anisotropic fluids within the framework of bodies with multiple natural configurations, J. Non-Newton. Fluid Mech. 99 (2001) 109–124.
- [36] K. Kannan, K. Rajagopal, Simulation of fiber spinning including flow-induced crystallization, J. Rheol. 49 (2005) 683–703.
- [37] T. McLeish, Tube theory of entangled polymer dynamics, Adv. Phys. 51 (2002) 1379–1527.
- [38] J.C.-W. Lee, K.M. Weigandt, E.G. Kelley, S.A. Rogers, Structure-property relationships via recovery rheology in viscoelastic materials, Phys. Rev. Lett. 122 (2019) 248003
- [39] M. Yamamoto, Rate-dependent relaxation spectra and their determination, Trans. Soc. Rheol. 15 (1971) 331–344.
- [40] M. Wagner, Analysis of time-dependent non-linear stress-growth data for shear and elongational flow of a low-density branched polyethylene melt, Rheol. Acta 15 (1976) 136–142.
- [41] M. Doi, S.F. Edwards, S.F. Edwards, The Theory of Polymer Dynamics, vol. 73, Oxford University Press, 1988.
- [42] M. Wagner, J. Meissner, Network disentanglement and time-dependent flow behaviour of polymer melts, Die Makromol. Chem. Macromol. Chem. Phys. 181 (1980) 1533–1550.
- [43] J.F. Berret, J. Appell, G. Porte, Linear rheology of entangled wormlike micelles, Langmuir 9 (1993) 2851–2854.
- [44] J.-F. Berret, D.C. Roux, G. Porte, Isotropic-to-nematic transition in wormlike micelles under shear, J. Phys. II 4 (1994) 1261–1279.
- [45] C. Pipe, N. Kim, P. Vasquez, L. Cook, G. McKinley, Wormlike micellar solutions: II. Comparison between experimental data and scission model predictions, J. Rheol. 54 (2010) 881–913.
- [46] P. Cheng, M.C. Burroughs, L.G. Leal, M.E. Helgeson, Distinguishing shear banding from shear thinning in flows with a shear stress gradient, Rheol. Acta 56 (2017) 1007–1032.
- [47] R.N. Al-kaby, J.S. Jayaratne, T.I. Brox, S.L. Codd, J.D. Seymour, J.R. Brown, Rheo-NMR of transient and steady state shear banding under shear startup, J. Rheol. 62 (2018) 1125–1134.
- [48] J. Läuger, A new rheometer platform for extended testing capabilities, Annu. Trans. Nord. Rheol. Soc. 21 (2013) 1–5.
- [49] R. Granek, M. Cates, Stress relaxation in living polymers: Results from a Poisson renewal model, J. Chem. Phys. 96 (1992) 4758–4767.

- [50] P.A. Vasquez, G.H. McKinley, L.P. Cook, A network scission model for wormlike micellar solutions: I. Model formulation and viscometric flow predictions, J. Non-Newton. Fluid Mech. 144 (2007) 122–139.
- [51] J.D. Ferry, Viscoelastic properties of polymer solutions, J. Res. Natl. Bur. Stand. 41 (1948) 53–62.
- [52] R.H. Ewoldt, G.H. Mckinley, Creep ringing in rheometry or how to deal with oft-discarded data in step stress tests! randy, Rheology 76 (2007).
- [53] C. Baravian, D. Quemada, Using instrumental inertia in controlled stress rheometry, Rheol. Acta 37 (1998) 223–233.
- [54] J. Dealy, Weissenberg and deborah numbers—their definition and use, Rheol. Bull. 79 (2010) 14–18.
- [55] J.L. White, Dynamics of viscoelastic fluids, melt fracture, and the rheology of fiber spinning. J. Appl. Polym. Sci. 8 (1964) 2339–2357.
- [56] S.-i. Ohta, Y. Einaga, K. Osaki, M. Kurata, Stress relaxation of polymer solutions under large strain: Elastic recovery after partial stress relaxation, Bull. Inst. Chem. Res. Kyoto Univ. 51 (1973) 220–230.
- [57] M. Fukuda, K. Osaki, M. Kurata, Nonlinear viscoelasticity of polystyrene solutions. I. Strain-dependent relaxation modulus, J. Polym. Sci. Polym. Phys. Ed. 13 (1975) 1563–1576.
- [58] R.L. Thompson, A.A. Alicke, P.R. de Souza Mendes, Model-based material functions for SAOS and LAOS analyses, J. Non-Newton. Fluid Mech. 215 (2015) 19–30.
- [59] M.M. Cross, Rheology of non-Newtonian fluids: A new flow equation for pseudoplastic systems, J. Colloid Sci. 20 (1965) 417–437.
- [60] T.E. Kusuma, P.J. Scales, R. Buscall, D.R. Lester, A.D. Stickland, Strain softening of concentrated cohesive particulate suspensions prior to yield, J. Rheol. 65 (2021) 355–370.
- [61] J. White, A. Metzner, Development of constitutive equations for polymeric melts and solutions, J. Appl. Polym. Sci. 7 (1963) 1867–1889.
- [62] M. Herrchen, H.C. Öttinger, A detailed comparison of various FENE dumbbell models, J. Non-Newton. Fluid Mech. 68 (1997) 17–42.
- [63] A. Zacharatos, E. Kontou, Nonlinear viscoelastic modeling of soft polymers, J. Appl. Polym. Sci. 132 (2015).
- [64] M.D. Monsia, A simplified nonlinear generalized Maxwell model for predicting the time dependent behavior of viscoelastic materials, 2011.
- [65] S.A. Rogers, J.D. Park, C.-W.J. Lee, Instantaneous dimensionless numbers for transient nonlinear rheology, Rheol. Acta 58 (2019) 539–556.
- [66] V.H. Rolón-Garrido, M.H. Wagner, The damping function in rheology, Rheol. Acta 48 (2009) 245–284.